

Propagation of thermal waves in multilayered spheres

Nora Madariaga and Agustín Salazar^{a)}

Departamento de Física Aplicada I, Escuela Técnica Superior de Ingeniería, Universidad del País Vasco, Alameda Urquijo s/n, 48013 Bilbao, Spain

(Received 6 February 2007; accepted 24 March 2007; published online 30 May 2007)

In the last years there has been a growing interest in the application of photothermal techniques to samples with nonflat surfaces, in particular cylinders and spheres. In this work the surface temperature oscillation of multilayered spherical samples which are heated by a modulated light beam is calculated by using the quadrupole method. Several illumination geometries have been studied. Moreover, the lack of adherence between layers, as well as heat losses at the surface, has been considered in the model. This theoretical approach allows photothermal techniques to be used to characterize the thermal properties of spherical samples with continuously varying in-depth thermal conductivity. © 2007 American Institute of Physics. [DOI: 10.1063/1.2735414]

I. INTRODUCTION

Photothermal techniques have become very powerful tools for the thermophysical characterization and nondestructive evaluation (NDE) of a wide variety of materials.¹ Photothermal-wave techniques are based on the generation and detection of thermal waves in the sample under study. Thermal waves are generated in a material as a consequence of the absorption of an intensity-modulated light beam. These highly damped thermal waves propagate through the material and are scattered by the buried heterogeneities. Different photothermal setups have been developed to detect these thermal waves and therefore to extract information on the thermal properties and internal structure of the material: infrared radiometry, mirage effect, photothermal reflectance, etc.

For decades, research in photothermal techniques has been restricted to samples with flat surfaces. Recently, some studies of cylindrical and spherical samples have been published.²⁻⁵ In this work we use the quadrupole method to calculate the surface temperature of a multilayered spherical sample which is heated by a modulated light beam. The quadrupole method is a unified exact method for representing linear systems. It has been applied in the framework of conductive transfer to calculate the surface temperature of multilayered flat samples⁶ and multilayered cylindrical samples.⁵ Here we exploit this elegant method to express the surface temperature of multilayered spherical samples in a compact manner. Different illumination geometries have been studied, both with and without keeping the spherical symmetry. On the other hand, the lack of adherence between layers has been taken into account by introducing a thermal contact resistance. Moreover, heat losses at the surface have also been considered. Consequently, it is expected that this theoretical approach encourages the use of photothermal techniques for the quantitative thermophysical characterization of spherical samples with continuously varying in-depth thermal conductivity, as is the case of hardened-steel ball bearings.

In Sec. II we first apply the quadrupole method to calculate the surface temperature of a multilayered sphere that is uniformly illuminated by a light beam modulated at a frequency f ($\omega=2\pi f$). Accordingly, in this simple configuration the one-dimensional approach can be used. Then, in Sec. III, we generalize the method to include nonuniform illuminations, which are of more practical interest.

II. MULTILAYERED SPHERE WITH UNIFORM ILLUMINATION

A. A hollow sphere

Let us consider a homogeneous and opaque hollow sphere with an outer radius a and an inner radius b , which is uniformly illuminated by a light beam of intensity I_0 modulated at a frequency f . Its cross section is shown in Fig. 1(a). Due to the spherical symmetry of the illumination, the temperature oscillation at any point of the sphere can be written as⁷

$$T(r) = Uj_0(qr) + Vh_0(qr), \tag{1}$$

where $q = \sqrt{i\omega/D}$ is the thermal wave vector, with D the thermal diffusivity of the sample, and j_0 and h_0 are the zeroth order of the spherical Bessel and Hankel functions, respectively. The first term in Eq. (1) represents the ingoing spheri-

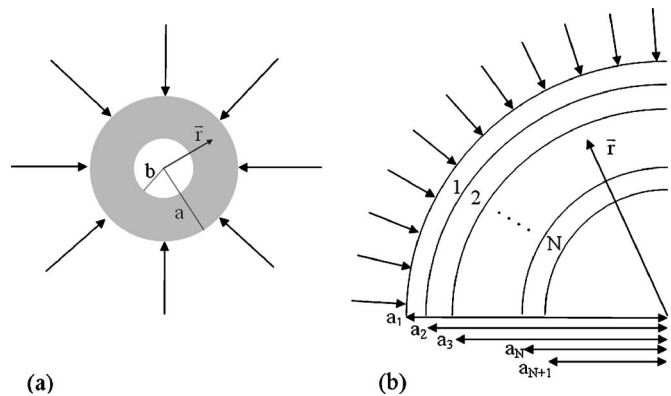


FIG. 1. Cross section of a hollow sphere (a) and a multilayered sphere (b) uniformly illuminated.

^{a)}Electronic mail: agustin.salazar@ehu.es

cal thermal wave starting at the sample surface, while the second one is the corresponding reflected wave at the inner surface. U and V are two constants to be determined according to the boundary conditions. On the other hand, if we define ϕ as minus the heat flux at any point of the sphere, then it is written

$$\phi(r) = K \frac{dT}{dr} = Kq [Uj_0'(qr) + Vh_0'(qr)], \quad (2)$$

where K is the thermal conductivity of the sample and j_0' and h_0' are the derivatives of the spherical Bessel and Hankel functions, respectively. The constants U and V can be easily eliminated from Eqs. (1) and (2) by taking the values of temperature and heat flux at both surfaces ($r=a$ and $r=b$). In this way, a linear relation between temperature and flux at the outer and inner surfaces is obtained, which can be expressed in the matrix form

$$\begin{pmatrix} T(a) \\ \phi(a) \end{pmatrix} = \begin{pmatrix} A & B \\ C & D \end{pmatrix} \begin{pmatrix} T(b) \\ \phi(b) \end{pmatrix}, \quad (3)$$

with

$$A = [h_0'(qb)j_0(qa) - j_0'(qb)h_0(qa)]/E,$$

$$B = [j_0(qb)h_0(qa) - h_0(qb)j_0(qa)]/EKq,$$

$$C = Kq[h_0'(qb)j_0'(qa) - j_0'(qb)h_0'(qa)]/E,$$

$$D = [j_0(qb)h_0'(qa) - h_0(qb)j_0'(qa)]/E,$$

$$E = h_0'(qb)j_0(qb) - h_0(qb)j_0'(qb).$$

It is interesting to note that Eq. (3) is valid for any boundary condition at the surfaces. According to Eq. (3), if the heat flux at both surfaces is known, then the surface temperature can be obtained. For instance, for negligible heat losses [$\phi(a)=I_0/2$ and $\phi(b)=0$] the surface temperature at both surfaces reduces to

$$T(a) = \frac{I_0 A}{2 C}, \quad (4a)$$

$$T(b) = \frac{I_0}{2 C}. \quad (4b)$$

On the other hand, when heat losses are present [$\phi(a)=I_0/2-H_a T(a)$ and $\phi(b)=H_b T(b)$] the surface temperature is written

$$T(a) = \frac{I_0}{2} \frac{A + BH_b}{C + DH_b + AH_a + BH_a H_b}, \quad (5a)$$

$$T(b) = \frac{I_0}{2} \frac{1}{C + DH_b + AH_a + BH_a H_b}, \quad (5b)$$

where H_a and H_b are the linearized heat transfer coefficients at the outer and inner surfaces, respectively, which account for convective and radiative losses.⁶ Note that in the absence of heat losses ($H_a=H_b=0$) Eqs. (5a) and (5b) reduce to Eqs. (4a) and (4b). On the other hand, by making $b=0$ in Eq. (5a) and using the properties of the spherical Bessel functions,^{8,9}

the surface temperature of a solid sphere is obtained:

$$T(a) = \frac{I_0}{2} \frac{j_0(qa)}{Kqj_0'(qa) + H_a j_0(qa)}. \quad (6)$$

As the radius of the sphere a tends to infinity, Eq. (6) reduces to $T(a)=(I_0/2)(1/Kq+H_a)$, which is the expression for the surface temperature of a semi-infinite flat sample with extended illumination.

It is worth noting that Eqs. (3), (4a), (4b), (5a), and (5b) are the same as those obtained for a homogeneous and semi-infinite slab and for a hollow cylinder whose front surfaces are periodically illuminated by a uniform light beam,^{5,6} but now the coefficients from A to D depend neither on hyperbolic functions nor on Bessel functions but on spherical Bessel functions. That is the reason why we have used minus the heat flux instead of the heat flux itself.

B. A multilayered sphere

Now we consider an opaque multilayered sphere whose outer surface is uniformly illuminated by a radial light beam of intensity I_0 modulated at a frequency f . Its cross section is shown in Fig. 1(b). It is made of N layers of different thicknesses and materials. The thermophysical properties of layer i are labeled by subindex i and its outer and inner radii by a_i and a_{i+1} , respectively. According to the quadrupole method the temperature at the outer and inner surfaces of the sphere, taking into account the influence of heat losses, is given by Eqs. (5a) and (5b):

$$T(a_1) = \frac{I_0}{2} \frac{A' + B'H_b}{C' + D'H_b + A'H_a + B'H_a H_b}, \quad (7a)$$

$$T(a_{N+1}) = \frac{I_0}{2} \frac{1}{C' + D'H_b + A'H_a + B'H_a H_b}, \quad (7b)$$

but now the transfer matrix to obtain the frequency-dependent coefficients $A'-D'$ is

$$\begin{pmatrix} A' & B' \\ C' & D' \end{pmatrix} = \prod_{i=1}^N \begin{pmatrix} A_i & B_i \\ C_i & D_i \end{pmatrix}, \quad (8)$$

with

$$A_i = [h_0'(q_i a_{i+1})j_0(q_i a_i) - j_0'(q_i a_{i+1})h_0(q_i a_i)]/E_i,$$

$$B_i = [j_0(q_i a_{i+1})h_0(q_i a_i) - h_0(q_i a_{i+1})j_0(q_i a_i)]/E_i K_i q_i,$$

$$C_i = K_i q_i [h_0'(q_i a_{i+1})j_0'(q_i a_i) - j_0'(q_i a_{i+1})h_0'(q_i a_i)]/E_i,$$

$$D_i = [j_0(q_i a_{i+1})h_0'(q_i a_i) - h_0(q_i a_{i+1})j_0'(q_i a_i)]/E_i,$$

$$E_i = h_0'(q_i a_{i+1})j_0(q_i a_{i+1}) - h_0(q_i a_{i+1})j_0'(q_i a_{i+1}).$$

On the other hand, the lack of adherence between two adjacent layers can be accounted for by considering a very thin intermediate air layer. The thickness of this intermediate layer satisfies the condition $\ell_n = a_n - a_{n+1} \rightarrow 0$, and according to the asymptotic behavior of the spherical Bessel functions,^{8,9} the coefficients of the corresponding transfer matrix can be simplified as $A_n = D_n = 1$, $B_n = \ell_n / K_{\text{air}} = R$, and

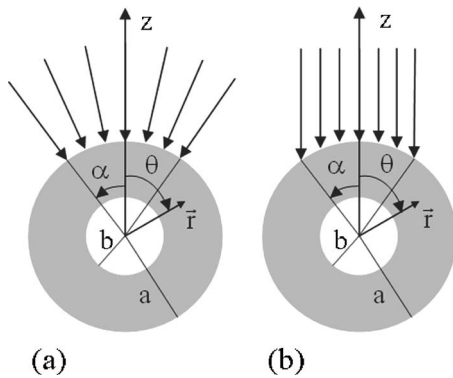


FIG. 2. Cross section of a hollow sphere with two kinds of nonuniform illumination: (a) radial and (b) flat.

$C_n=0$. Here R is the thermal contact resistance. This means that the effect of a thermal resistance between layers i and $i+1$ ($R_{i,i+1}$) is accounted for by inserting in Eq. (8) the following matrix between the two adjacent matrices i and $i+1$:

$$\begin{pmatrix} 1 & R_{i,i+1} \\ 0 & 1 \end{pmatrix}. \quad (9)$$

III. MULTILAYERED SPHERE WITH NONUNIFORM ILLUMINATION

The illumination we dealt with in the previous section is the easiest one to be solved mathematically because of the spherical symmetry. However, this is difficult to fulfill in photothermal experiments. Accordingly, we generalize the thermal quadrupole procedure to include two types of illumination with no spherical symmetry, but with more practical applications: radial and flat geometries (see Fig. 2). Both subtend the same angle $\theta=\alpha$. In the first one [see Fig. 2(a)] the light intensity over the sphere surface $g(\theta, \alpha)$ is I_0 for $0 \leq \theta \leq \alpha$ and zero for all other angles, and after being expanded in Fourier-Legendre series is written⁹

$$g(\theta, \alpha) = I_0 \sum_{n=0}^{\infty} \left(\frac{2n+1}{2} \int_0^\alpha P_n(\cos \lambda) \sin \lambda d\lambda \right) \times P_n(\cos \theta) = I_0 \sum_{n=0}^{\infty} g_n(\alpha) P_n(\cos \theta), \quad (10)$$

where P_n are the Legendre polynomials.

In the second one [see Fig. 2(b)] the light intensity is $I_0 \cos \theta$ for $0 \leq \theta \leq \alpha$ and zero for all other angles, and expanded in Fourier series can be written as

$$g(\theta, \alpha) = I_0 \sum_{n=0}^{\infty} \left(\frac{2n+1}{2} \int_0^\alpha P_n(\cos \lambda) \cos \lambda \sin \lambda d\lambda \right) \times P_n(\cos \theta) = I_0 \sum_{n=0}^{\infty} g_n(\alpha) P_n(\cos \theta). \quad (11)$$

A. A hollow sphere

Let us consider the same hollow sphere as in Sec. II A. Two light beams are considered whose cross-sections are shown in Fig. 2. According to the loss of spherical symmetry, the temperature oscillation at any point of the sphere is given by⁷

$$T(r, \theta) = \sum_{n=0}^{\infty} [U_n j_n(qr) + V_n h_n(qr)] P_n(\cos \theta) = \sum_{n=0}^{\infty} t_n(r) P_n(\cos \theta), \quad (12)$$

where j_n and h_n are the n th order of the spherical Bessel and Hankel functions, respectively. U_n and V_n are constants to be determined according to the boundary conditions. On the other hand, ϕ at any point of the sphere is written

$$\phi(r, \theta) = K \frac{\partial T}{\partial r} = Kq \sum_{n=0}^{\infty} [U_n j'_n(qr) + V_n h'_n(qr)] P_n(\cos \theta) = \sum_{n=0}^{\infty} f_n(r) P_n(\cos \theta), \quad (13)$$

where j'_n and h'_n are the derivatives of the Bessel and Hankel functions, respectively. The U_n and V_n constants can be eliminated from Eqs. (12) and (13) by taking the values of t_n and f_n at both surfaces ($r=a$ and $r=b$). In this way, a linear relation between t_n and f_n at the outer and inner surfaces is obtained, which can be expressed in the matrix form

$$\begin{pmatrix} t_n(a) \\ f_n(a) \end{pmatrix} = \begin{pmatrix} A_n & B_n \\ C_n & D_n \end{pmatrix} \begin{pmatrix} t_n(b) \\ f_n(b) \end{pmatrix}, \quad \forall n=0, \dots, \infty, \quad (14)$$

with

$$\begin{aligned} A_n &= [h'_n(qb)j_n(qa) - j'_n(qb)h_n(qa)]/E_n, \\ B_n &= [j_n(qb)h_n(qa) - h_n(qb)j_n(qa)]/E_n Kq, \\ C_n &= Kq[h'_n(qb)j'_n(qa) - j'_n(qb)h'_n(qa)]/E_n, \\ D_n &= [j_n(qb)h'_n(qa) - h_n(qb)j'_n(qa)]/E_n, \\ E_n &= h'_n(qb)j_n(qb) - h_n(qb)j'_n(qb). \end{aligned}$$

For negligible heat losses [$f_n(a)=I_0 g_n(\alpha)/2$ and $f_n(b)=0$, $\forall n=0, \dots, \infty$] the coefficients $t_n(a)$ and $t_n(b)$ are

$$t_n(a) = \frac{I_0}{2} g_n(\alpha) \frac{A_n}{C_n}, \quad (15a)$$

$$t_n(b) = \frac{I_0}{2} g_n(\alpha) \frac{1}{C_n}, \quad (15b)$$

and using Eq. (12) the surface temperature can be obtained:

$$T(a, \theta) = \frac{I_0}{2} \sum_{n=0}^{\infty} g_n(\alpha) \frac{A_n}{C_n} P_n(\cos \theta), \quad (16a)$$

$$T(b, \theta) = \frac{I_0}{2} \sum_{n=0}^{\infty} g_n(\alpha) \frac{1}{C_n} P_n(\cos \theta), \quad (16b)$$

where $g_n(\alpha)$ is taken from Eqs. (10) or (11) according to the geometry of the illumination.

When heat losses are present [$f_n(a) = I_0 g_n(\alpha) / 2 - H_a t_n(a)$ and $f_n(b) = H_a t_n(b)$, $\forall n = 0, \dots, \infty$] the coefficients $t_n(a)$ and $t_n(b)$ are

$$t_n(a) = \frac{I_0}{2} g_n(\alpha) \frac{A_n + B_n H_b}{C_n + D_n H_b + A_n H_a + B_n H_a H_b}, \quad (17a)$$

$$t_n(b) = \frac{I_0}{2} g_n(\alpha) \frac{1}{C_n + D_n H_b + A_n H_a + B_n H_a H_b}, \quad (17b)$$

and from Eq. (12) the surface temperature is obtained:

$$T(a, \theta) = \frac{I_0}{2} \sum_{n=0}^{\infty} g_n(\alpha) \frac{A_n + B_n H_b}{C_n + D_n H_b + A_n H_a + B_n H_a H_b} \times P_n(\cos \theta), \quad (18a)$$

$$T(b, \theta) = \frac{I_0}{2} \sum_{n=0}^{\infty} g_n(\alpha) \frac{1}{C_n + D_n H_b + A_n H_a + B_n H_a H_b} \times P_n(\cos \theta). \quad (18b)$$

As a particular case, by making $b=0$ in Eq. (18a) and using the properties of the spherical Bessel functions,^{8,9} a simple expression for the surface temperature of a solid sphere is obtained:

$$T(a, \theta) = \frac{I_0}{2} \sum_{n=0}^{\infty} g_n(\alpha) \frac{j_n(qa)}{Kqj_n'(qa) + H_a j_n(qa)} P_n(\cos \theta). \quad (19)$$

B. A multilayered sphere

Finally, we consider the same multilayered sphere as in Sec. II B. Proceeding in a similar way as before, the temperature at any point of the outer and inner surfaces, taking into account the influence of heat losses, is given by Eqs. (18a) and (18b):

$$T(a_1, \theta) = \frac{I_0}{2} \sum_{n=0}^{\infty} g_n(\alpha) \frac{A'_n + B'_n H_b}{C'_n + D'_n H_b + A'_n H_a + B'_n H_a H_b} \times P_n(\cos \theta), \quad (20a)$$

$$T(a_{N+1}, \theta) = \frac{I_0}{2} \sum_{n=0}^{\infty} g_n(\alpha) \frac{1}{C'_n + D'_n H_b + A'_n H_a + B'_n H_a H_b} \times P_n(\cos \theta), \quad (20b)$$

but now the n transfer matrices to obtain the frequency-dependent coefficients $A'_n - D'_n$ are

$$\begin{pmatrix} A'_n & B'_n \\ C'_n & D'_n \end{pmatrix} = \prod_{i=1}^N \begin{pmatrix} A_{ni} & B_{ni} \\ C_{ni} & D_{ni} \end{pmatrix}, \quad n = 0, \dots, +\infty, \quad (21)$$

with

$$A_{ni} = [h'_{ni}(q_i a_{i+1}) j_{ni}(q_i a_i) - j'_{ni}(q_i a_{i+1}) h_{ni}(q_i a_i)] E_{ni},$$

$$B_{ni} = [j_{ni}(q_i a_{i+1}) h_{ni}(q_i a_i) - h_{ni}(q_i a_{i+1}) j_{ni}(q_i a_i)] / E_{ni} K_i q_i,$$

$$C_{ni} = K_i q_i [h'_{ni}(q_i a_{i+1}) j'_{ni}(q_i a_i) - j'_{ni}(q_i a_{i+1}) h'_{ni}(q_i a_i)] / E_{ni},$$

$$D_{ni} = [j_{ni}(q_i a_{i+1}) h'_{ni}(q_i a_i) - h_{ni}(q_i a_{i+1}) j'_{ni}(q_i a_i)] / E_{ni},$$

$$E_{ni} = h'_{ni}(q_i a_{i+1}) j_{ni}(q_i a_{i+1}) - h_{ni}(q_i a_{i+1}) j'_{ni}(q_i a_{i+1}).$$

As in the case of illumination with spherical symmetry, the influence of a bad adherence between layers i and $i+1$ is accounted for by inserting in Eq. (21) the same matrix given by Eq. (9) between the two adjacent matrices i and $i+1$.

IV. NUMERICAL CALCULATIONS AND DISCUSSION

Before starting with the study of multilayered spheres, we performed two tests of consistency. First, we calculated the surface temperature of a solid multilayered sphere made of four layers of different thicknesses, but with the same thermal properties. Calculations have been performed for different values of the thermal properties and thicknesses. In the case of uniform illumination [see Fig. 1(b)] we have used Eq. (7a) and the amplitude and phase of the temperature are always the same as those calculated for a solid sphere using Eq. (6). In the same way, for the case of flat illumination [see Fig. 2(b)] we have used Eq. (20a) and the results are always the same as those obtained for a solid sphere with Eq. (19). Second, we calculated the surface temperature of a hollow sphere using Eqs. (4a) and (4b) when a and b tend to infinity. We have used different values of the thermal properties of the hollow sphere and the obtained amplitude and phase of the surface temperature are always the same as those obtained for a flat slab with thickness $l = a - b$.

We first present some numerical simulations for the case of uniform illumination. As an illustrative example we calculate the surface temperature oscillation in a two-layer solid sphere with a total radius of 1 mm. The outer layer is made of AISI-304 stainless steel ($K = 15 \text{ W m}^{-1} \text{ K}^{-1}$ and $D = 4 \text{ mm}^2/\text{s}$) with a thickness of 0.2 mm. In all the simulations the surface temperature of the two-layer sphere is normalized to a solid stainless-steel sphere with the same radius as the bilayer one. In Fig. 3 the influence of the material of the inner layer on the amplitude and phase of the surface temperature is shown as a function of the modulation frequency. Calculations have been performed using Eq. (7a) with no heat losses. Four cases have been considered: (a) an extremely good thermal conductor ($K = 1000 \text{ W m}^{-1} \text{ K}^{-1}$ and $D = 100 \text{ mm}^2/\text{s}$),¹⁰ (b) copper ($K = 400 \text{ W m}^{-1} \text{ K}^{-1}$ and $D = 116 \text{ mm}^2/\text{s}$), (c) a typical polymer ($K = 0.25 \text{ W m}^{-1} \text{ K}^{-1}$ and $D = 0.10 \text{ mm}^2/\text{s}$), and (d) air ($K = 0.026 \text{ W m}^{-1} \text{ K}^{-1}$ and $D = 22 \text{ mm}^2/\text{s}$). As can be seen, at high frequencies the normalized amplitude tends to 1, indicating that the thermal

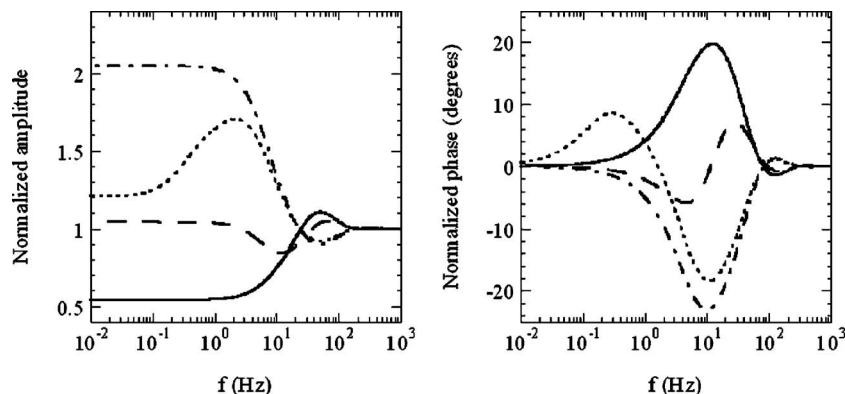


FIG. 3. Normalized amplitude and phase of the surface temperature of a two-layer sphere whose radius is 1 mm, and with a uniform illumination. The outer layer is 0.2 mm thick made of AISI-304 stainless steel. Four different inner layers have been considered: (a) an extremely good thermal conductor, solid line, (b) copper, dashed line, (c) a polymer, dotted line, and (d) air, dash-dotted line.

wave does not reach the inner core. As the frequency decreases the normalized amplitude is higher (smaller) than 1 if the thermal effusivity ($e=K/\sqrt{D}$) of the inner core is lower (higher) than that of the outer layer. This is due to the fact that the reflected thermal wave at the interface is in phase (out of phase) with respect to the incident one, giving rise to a constructive (destructive) interference. Finally, at very low frequencies the sphere becomes thermally thin and its surface temperature, which is given by Eq. (6), reduces to

$$T(a) \approx \frac{I_0}{2} \frac{3}{\omega \rho c a} \exp\left(-i \frac{\pi}{2}\right), \tag{22}$$

indicating that the amplitude of the surface temperature depends on the inverse of the heat capacity ($\rho c=K/D$, where ρ is the density and c the specific heat) while the phase remains constant (-90°). Accordingly, at very low frequencies the normalized temperature T_n of the two-layer sphere is written

$$T_n \approx \frac{(\rho c)_{\text{solid sphere}}}{(\rho c)_{\text{two layer}}} = \frac{(\rho c)_{\text{solid sphere}}}{v_1(\rho c)_{\text{outer layer}} + v_2(\rho c)_{\text{inner layer}}}, \tag{23}$$

where v_1 and v_2 are the volume fractions of the outer layer and the inner core, respectively. In our calculations $v_1=0.488$ and $v_2=0.512$. This means that for the extremely good thermal conductor ($\rho c=10 \times 10^6$ S.I.) $T_n=0.54$, for copper ($\rho c=3.45 \times 10^6$ S.I.) $T_n=1.04$, for the polymer ($\rho c=2.5 \times 10^6$ S.I.) $T_n=1.21$, and for air ($\rho c=1.18 \times 10^3$ S.I.) $T_n=2.05$, which are exactly the low-frequency values in Fig. 3.

On the other hand, at high frequencies the normalized phase tends to 0, but as the frequency decreases the normal-

ized phase is positive (negative) when the thermal effusivity of the inner core is higher (lower) than that of the outer layer. This is valid when the thermal effusivities of the two layers are very different (see the solid and dash-dotted lines in Fig. 3). If it is not the case, the normalized phase shows an oscillation, changing from positive to negative when the inner core has a lower effusivity than the outer layer and from negative to positive if the inner core has a higher effusivity than the outer layer. Finally, at very low frequencies the normalized phase tends to 0 since both the solid sphere and the two-layer one are thermally thin and in such a case the phase is independent of the thermal properties [see Eq. (22)]. It is worth noting that all these results are similar to those found in two-layer flat materials and in two-layer solid cylinders (see, for instance, Fig. 3 in Ref. 5). The main difference is that for the same materials and sizes the phase contrast becomes smaller for the sphere than for the cylinder.

The influence on the surface temperature due to the presence of a thermal resistance between the two layers is shown in Fig. 4. The material is the same two-layer solid sphere as in Fig. 3 with the inner layer made of copper. Calculations have been performed using Eq. (7a) with no heat losses. The solid line represents a perfect thermal contact, the dashed line is for $R=10^{-5} \text{ m}^2 \text{ K W}^{-1}$, the dotted line is for $R=10^{-4} \text{ m}^2 \text{ K W}^{-1}$, and the dash-dotted line is for $R=10^{-3} \text{ m}^2 \text{ K W}^{-1}$. As the thermal resistance increases both amplitude and phase differ from the perfect thermal contact and the temperature behaves as in the case of an inner thermal insulator: the normalized amplitude increases and the normalized phase changes from negative to positive (see the dotted line in Fig. 3 corresponding to the polymer). In Fig. 5

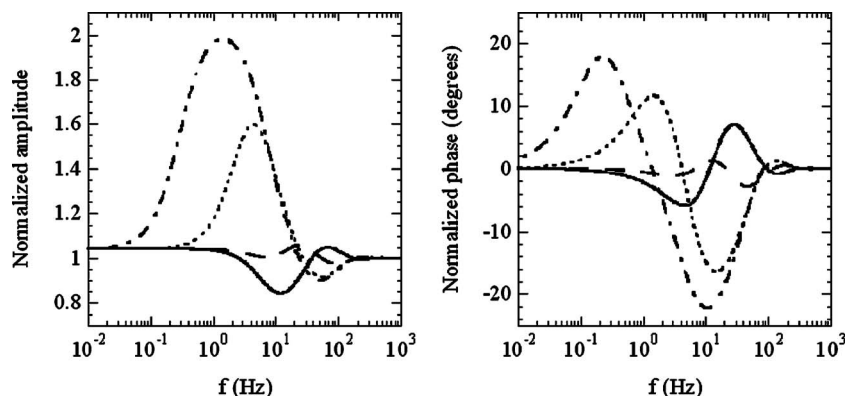


FIG. 4. Effect of the thermal resistance in the normalized amplitude and phase of the surface temperature of a two-layer sphere whose radius is 1 mm and with a uniform illumination. The outer layer is 0.2 mm thick made of AISI-304 stainless steel. The inner layer is made of copper. (a) $R=0$, solid line, (b) $R=10^{-5} \text{ m}^2 \text{ K W}^{-1}$, dashed line, (c) $R=10^{-4} \text{ m}^2 \text{ K W}^{-1}$, dotted line, and (d) $R=10^{-3} \text{ m}^2 \text{ K W}^{-1}$, dash-dotted line.

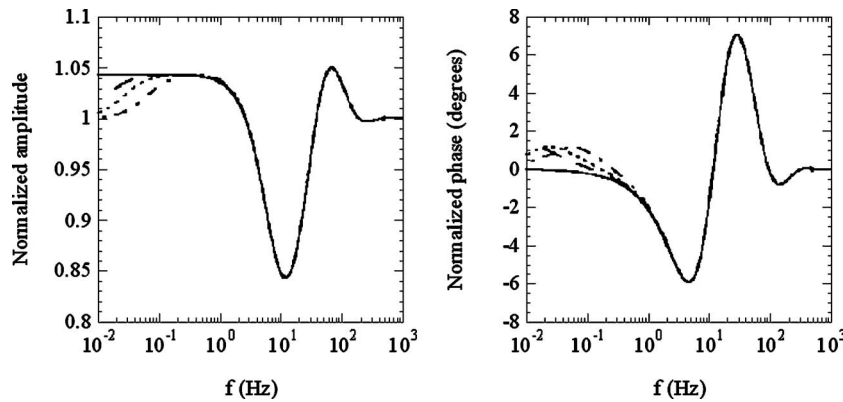


FIG. 5. Effect of heat losses in the normalized amplitude and phase of the surface temperature for the same two-layer sphere as in Fig. 4. (a) $H=0$, solid line, (b) $H=100 \text{ W m}^{-2} \text{ K}^{-1}$, dashed line, (c) $H=200 \text{ W m}^{-2} \text{ K}^{-1}$, dotted line, and (d) $H=500 \text{ W m}^{-2} \text{ K}^{-1}$, dash-dotted line.

the influence of heat losses at the surface is shown. The bilayer sphere is the same as in Fig. 4, with a perfect thermal contact between core and coating. The solid line represents the absence of heat losses, and it is the same curve as the solid line in Fig. 4. The influence of heat losses only appears at very low frequencies, and it is small even for high coefficients of heat losses ($H=100\text{--}500 \text{ W m}^{-2} \text{ K}^{-1}$). This is due to the fact that stainless steel is quite a good thermal conductor and the influence of heat losses increases as the thermal conductivity of the material decreases.

Following with the same uniform illumination we analyze the surface temperature of a solid multilayered sphere. It has a radius of 1 mm, with an inner core of radius 0.5 mm made of AISI-304 stainless steel ($K=15 \text{ W m}^{-1} \text{ K}^{-1}$ and $D=4 \text{ mm}^2/\text{s}$). In the outer part of the sphere the transport thermal properties suffer from a continuously steplike decrease down to half of the core values at the surface ($K=7.5 \text{ W m}^{-1} \text{ K}^{-1}$ and $D=2 \text{ mm}^2/\text{s}$), while keeping constant the heat capacity ($\rho c=3.75 \times 10^6 \text{ S.I.}$). Calculations have been performed using Eq. (7a) with no heat losses. In Fig. 6 the normalized amplitude and phase of the surface temperature oscillation is shown as a function of the modulation frequency. Normalization is performed with respect to a homogeneous sphere of the same size made of AISI-304 stainless steel. Four cases have been considered: (a) two outer layers 0.25 mm thick each, (b) three outer layers 0.166 mm thick each, (c) five outer layers 0.10 mm thick each, and (d) ten outer layers 0.05 mm thick each. It is seen that, at low frequencies, the normalized amplitude tends to 1 and the normalized phase tends to 0, according to Eq. (23) and taking into account that the heat capacities of the solid sphere and the multilayered one are the same. In contrast, at high

frequencies the surface temperature is proportional to the inverse of the thermal effusivity, since Eq. (6) reduces to

$$T(a) \approx \frac{I_0}{2} \frac{1}{e\sqrt{\omega}} \exp\left(-i\frac{\pi}{4}\right), \quad (24)$$

the same expression as for a flat sample, and therefore the normalized amplitude is given by

$$T_n \approx \frac{e_{\text{solid sphere}}}{e_{\text{outer layer}}}. \quad (25)$$

Accordingly, in our example $T_n=7500/5303=1.414$, which is the high-frequency value in Fig. 6. At intermediate frequencies there is a positive phase contrast since thermal waves propagating through the multilayered sphere are crossing layers of increasing effusivity and therefore the reflected thermal waves interfere destructively with the incident ones, as happened in Fig. 3 for an inner layer of copper (see the solid line). On the other hand, as the number of layers increases the shapes of both the amplitude and phase are similar but shifted to higher frequencies. Moreover, the highest phase contrast is reduced. This is due to the fact that as the number of layers increases the thermal contrast reduces and therefore the amplitude of the reflected thermal wave becomes smaller. Note that as the number of layers tends to infinity this model simulates the case of a heterogeneous sphere with continuously varying thermal properties, as is the case of samples affected by surface modifying processes—e.g., steel hardening, annealing, etc. However, as in the case of multilayered cylinders, the convergence is very slow and many layers are necessary to guarantee convergence at high frequencies.⁵

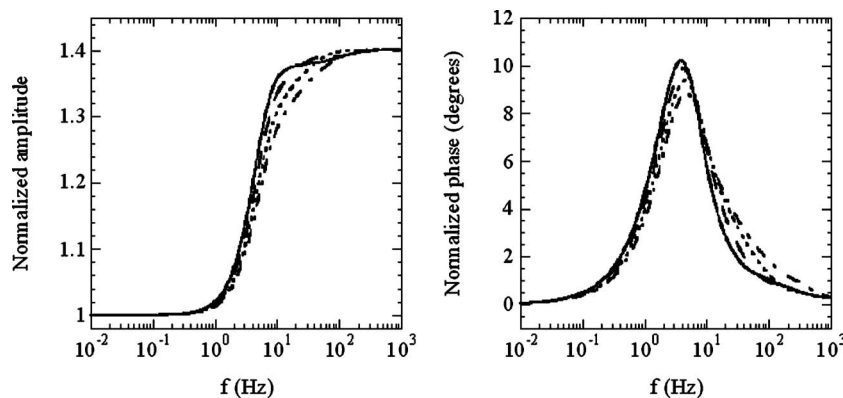


FIG. 6. Normalized amplitude and phase of the surface temperature of a multilayered sphere whose radius is 1 mm and with a uniform illumination. The inner core is made of AISI-304 stainless steel and has a radius of 0.5 mm. In the outer part of the sphere the transport thermal properties suffer from a continuously steplike decrease down to half of the core values at the surface. Four cases are considered: (a) two outer layers, solid line, (b) three outer layers, dashed line, (c) five outer layers, dotted line, and (d) ten outer layers, dash-dotted line.

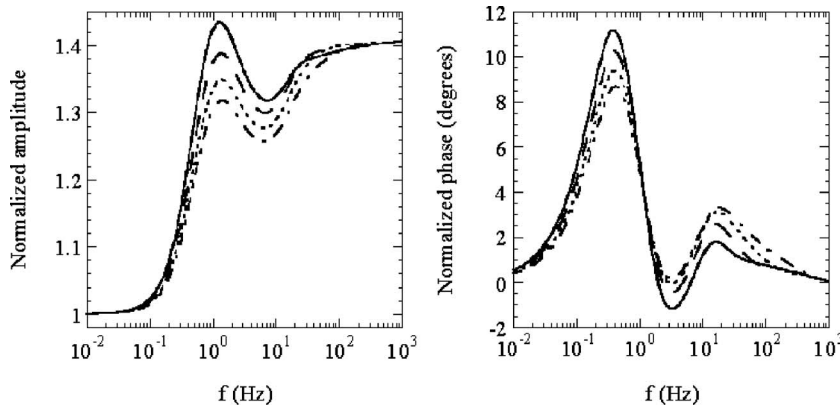


FIG. 7. The same as in Fig. 6, but now illuminated by a flat light beam, as that shown in Fig. 2(b), with $\alpha = \pi/2$. The temperature is calculated at the north pole of the sample ($\theta = 0$).

Now we study the same multilayered sphere of Fig. 6 but illuminated with a flat light beam [as that shown in Fig. 2(b)] with $\alpha = \pi/2$. Calculations have been performed using Eq. (20a) without heat losses. In Fig. 7 we show the frequency scan of the normalized amplitude and phase of the surface temperature as measured at the north pole of the sample ($\theta = 0$). Three differences with respect to Fig. 6 can be pointed out: (a) A double-peak structure appears in both the amplitude and phase, (b) a shift to lower frequencies of the features occurs, and (c) there is a small increase of the phase contrast.

It is worth noting that using the inverse Laplace transform,⁶ the modulated solutions presented in Secs. II and III can be used to calculate the temperature evolution of multilayered spheres after being heated by a short-duration light pulse. This means that this theoretical approach can be used in both lock-in and pulsed infrared thermography.

In this work an extension of the thermal quadrupole method to calculate the surface temperature of multilayered spherical samples has been presented. It is expected that this theoretical approach will encourage the use of photothermal techniques for quantitative thermophysical characterization of coated spheres and hardened-steel spherical samples such as ball bearings.

ACKNOWLEDGMENTS

This work has been supported by the Ministerio de Educación y Ciencia through research grant No. MAT2005-02999 and by the Universidad del País Vasco through research grant No. DIPE06/06. Nora Madariaga acknowledges a predoctoral fellowship from Ministerio de Educación y Ciencia (FPI).

¹D. P. Almond and P. M. Patel, *Photothermal Science and Techniques* (Chapman and Hall, London, 1996).

²C. Wang, A. Mandelis, and Y. Liu, *J. Appl. Phys.* **96**, 3756 (2004).

³C. Wang, A. Mandelis, and Y. Liu, *J. Appl. Phys.* **97**, 014911 (2005).

⁴A. Salazar, F. Garrido, and R. Celorrio, *J. Appl. Phys.* **99**, 066116 (2006).

⁵A. Salazar and R. Celorrio, *J. Appl. Phys.* **100**, 113535 (2006).

⁶D. Maillat, S. André, J. C. Batsale, A. Degiovanni, and C. Moyne, *Thermal Quadrupoles* (Wiley, New York, 2000).

⁷N. B. Kakogiannos and J. A. Roumeliotis, *J. Acoust. Soc. Am.* **98**, 3508 (1995).

⁸*Handbook of Mathematical Functions*, edited by M. A. Abramowitz and I. A. Stegun (National Bureau of Standards, Washington, DC, 1964).

⁹G. Arfken and H. J. Weber, *Mathematical Methods for Physicists*, 6th ed. (Academic Press, New York, 2005).

¹⁰This combination of K and D is unrealistic. It has been introduced to simulate a material with very high thermal effusivity and heat capacity, just the opposite of the air, which has very low effusivity and heat capacity.